 doi:10.20944/preprints202103.0662.v1

Article

A gadolinium(III) complex based on the thymine nucleobase with properties suitable for magnetic resonance imaging applications

Marta Orts-Arroyo [1], Amadeo Ten-Esteve [2], Sonia Ginés-Cárdenas [2], Isabel Castro [1], Luis Martí-Bonmatí [2,*] and José Martínez-Lillo [1,*]

[1] Instituto de Ciencia Molecular (ICMol), Universitat de València, c/ Catedrático José Beltrán 2, 46980 Paterna, València, Spain; e-mail: f.jose.martinez@uv.es
[2] Radiology Department and Biomedical Imaging Research Group (GIBI230), La Fe University and Polytechnic Hospital and La Fe Health Research Institute, Valencia, Spain; e-mail: marti_lui@gva.es
* Correspondence: f.jose.martinez@uv.es; Tel.: +34-9635-44460

Abstract:

The paramagnetic gadolinium(III) ion is used as contrast agent in magnetic resonance (MR) imaging to improve the lesion detection and characterization. It generates a signal by changing the relaxivity of protons from associated water molecules and creates a clearer physical distinction between the molecule and the surrounding tissues. New gadolinium-based contrast agents displaying larger relaxivity values and specifically targeted might provide higher resolution and better functional images. We have synthesized the gadolinium(III) complex of formula $[Gd(thy)_2(H_2O)_6](ClO_4)_3{\cdot}2H_2O$ (**1**) [thy = 5-methyl-1H-pyrimidine-2,4-dione or thymine], which is the first reported compound based on gadolinium and thymine nucleobase. **1** has been characterized through vis-IR, SEM-EDAX and single-crystal X-ray diffraction techniques, and its magnetic and relaxometric properties have been investigated by means of SQUID magnetometer and MR imaging phantom studies, respectively. On the basis of its high relaxivity values, this gadolinium(III) complex can be considered a suitable candidate for contrast enhanced magnetic resonance imaging.

Keywords: thymine; gadolinium; contrast agent; magnetic resonance; metal complexes; crystal structure; relaxivity

1. Introduction

Thymine is one of the four natural nitrogen bases that are precursors and part of the structure of the deoxyribonucleic acid (DNA) macromolecule [1,2]. This pyrimidine base has been widely studied, in part because of the common mutations of DNA caused when adjacent thymines are irradiated by UV light and are dimerized, generating the well-known thymine dimers [2,3]. Besides, considerable effort has also been devoted to the rational design of drugs that might selectively inhibit thymine biosynthesis, thereby blocking DNA replication, especially in rapidly dividing malignant cells.

In comparison with other natural nucleobases, the coordination chemistry of thymine-based metal complexes has been much less investigated. Most of the thymine-containing complexes have been prepared with the nucleobase in form of thyminate anion, that is, releasing one or two protons of its N-H groups, whereas the reported examples obtained with the thymine molecule acting through its carbonyl groups as a neutral ligand toward the metal are much scarcer [4-7]. In that respect, theoretical studies have been performed on metal clusters to investigate preferential binding sites of the thymine molecule [8].

Preprints (www.preprints.org) | NOT PEER-REVIEWED | Posted: 26 March 2021 doi:10.20944/preprints202103.0662.v1

There exist some published thymine-based complexes that exhibit singular properties, as for instance the Ru^{II}-thymine complex $[Ru(PPh_3)_2(thy)(bpy)]PF_6$ [where PPh_3 = triphenylphosphine and bpy = 2,2′-bipyridine], which is a potent cytotoxic agent with ability to bind to DNA inducing apoptotic cell death in human colon carcinoma [6,7]. Thymine has also shown to be a highly specific ligand towards Hg^{II} metal ion [9,10]. The discovery of the linear thymine-Hg^{II}-thymine structure, which affords a high stabilization of thymine-thymine pairs in DNA, has led to the designing and development of recent thymine-based sensors [11-13].

Regarding lanthanide complexes, only two structures based on thyminate anion have been published so far, namely, the heteropolynuclear complexes of general formula $[\{Cp^*Rh^{III}(\mu\text{-thym})\}_4\{Ln^{III}(NO_3)_2\}]^+$, where Ln = Dy^{III} and Er^{III}, which form cationic metallacalix[4]arene-type systems [14]. Hence, no crystal structure of gadolinium complex based on thymine has been reported up to date.

As continuation of our interest in investigating biomolecule-based complexes [15-20], herein we report the synthesis and characterization of a new gadolinium(III) complex of formula $[Gd(thy)_2(H_2O)_6](ClO_4)_3{\cdot}2H_2O$ (**1**) [thy = thymine], which exhibits a linearly disposed thymine-Gd^{III}-thymine structure (Fig. 1). Remarkably, **1** is the first reported compound based on gadolinium and thymine, as well as a suitable candidate for contrast enhanced magnetic resonance (MR) imaging applications.

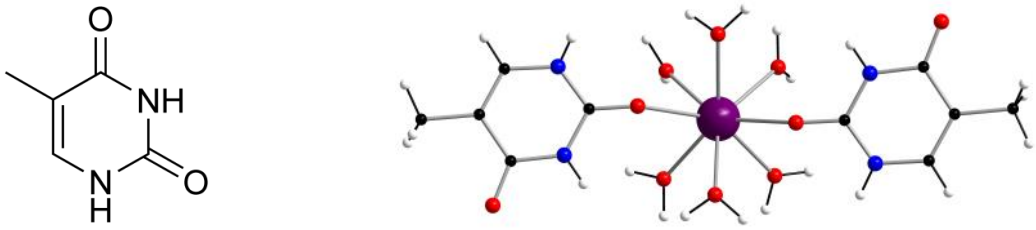

(**a**) (**b**)

Figure 1. (**a**) Molecular structure of the thymine nucleobase (thy); (**b**) Mononuclear $[Gd(thy)_2(H_2O)_6]^{3+}$ complex in **1**. ClO_4^- anions and non-coordinated water molecules have been omitted for clarity. Color code: purple, Gd; red, O; blue, N; black, C; white, H.

2. Materials and Methods

2.1. Reagents and Instruments

All of the manipulations were performed under aerobic conditions. All the commercial chemicals were used as received. CAUTION!: Although no problems were encountered in this work, care should be taken when using the potentially explosive perchlorate anion (ClO_4^-).

Elemental analyses (C, H, N) and X-ray microanalysis were performed by the Central Service for the Support to Experimental Research (SCSIE) at the University of Valencia. Scanning electron microscopy (SEM) images and results were obtained from a Hitachi S-4800 field emission scanning electron microscope. Infrared spectrum (IR) of **1** was recorded with a PerkinElmer Spectrum 65 FT-IR spectrometer in the range of 400 to 4000 cm^{-1}. Variable-temperature, solid-state direct current (DC) magnetic susceptibility data down to 2.0 K were collected on a Quantum Design MPMS-XL SQUID magnetometer (Quantum Design, Inc., San Diego, CA, USA) equipped with a 5 T DC magnet. The experimental magnetic data were corrected for the diamagnetic contributions of the constituent atoms and also for the sample holder. Data were collected on a Philips Achieva 3T clinical MR scanner with a volumetric head 8 channels SENSE coil at La Fe University and Polytechnic Hospital.

2.2. Preparation of compound **1**

Preprints (www.preprints.org) | NOT PEER-REVIEWED | Posted: 26 March 2021 doi:10.20944/preprints202103.0662.v1

2.2.1. Synthesis of $[Gd(thy)_2(H_2O)_6](ClO_4)_3{\cdot}2H_2O$ (**1**)

A mixture of Gd_2O_3 (0.091 g, 0.25 mmol) and thymine (0.063 g, 0.50 mmol) in an aqueous suspension (5 mL) was acidulated with perchloric acid (1.0 mL, 2 M) and was stirred and heated at 60 °C for 1h. The resulting solution was left to evaporate at room temperature for 1 week. Colorless parallelepipeds were obtained and were suitable for single-crystal X-ray diffraction studies. Yield: *ca*. 45%. Anal. Calcd. for $C_{10}H_{28}N_4O_{24}Cl_3Gd$ (**1**): C, 14.1; H, 3.3; N, 6.6. Found: C, 14.2; H, 3.0; N, 6.1. SEM-EDAX: a molar ratio of 1:3 for Gd/Cl was found for **1**. IR (KBr pellet/cm^{-1}): peaks are observed at 3399 (br), 3218 (m), 3063 (m), 2928 (m), 2813 (m), 1747 (s), 1678 (vs), 1635 (m), 1483 (w), 1449 (m), 1427 (w), 1383 (m), 1246 (m), 1205 (m), 1145 (vs), 1112 (vs), 1089 (vs), 935 (m), 835 (m), 815 (m), 760 (m), 744 (m), 627 (vs), 560 (m), 477 (m), 432 (m).

2.3. X-ray Data Collection and Structure Refinement

X-ray diffraction data from a single crystal of **1** with dimensions 0.34 × 0.12 × 0.05 mm^3 was collected on a Bruker D8 Venture diffractometer with graphite-monochromated Mo-K_α radiation (λ = 0.71073 Å). The structures were solved by standard direct methods and subsequently completed by Fourier recycling by using the SHELXTL software packages. The obtained model was refined with version 2018/1 of SHELXL against F^2 on all data by full-matrix least squares [21]. All non-hydrogen atoms were anisotropically refined, whereas the hydrogen atoms of the thymine molecules were set in calculated positions and refined isotropically by using the riding model. The graphical manipulations were performed with the DIAMOND program [22]. The CCDC code for **1** is 2009091.

3. Results and Discussion

3.1. Synthetic Procedure

Compound **1** is prepared from a mixture of Gd_2O_3 and thymine, which reacts in an aqueous suspension acidulated with perchloric acid, and is stirred at 60 °C for 1h. The resulting solution is left to evaporate at room temperature for 1 week, thus generating colorless parallelepipeds of **1**. Once synthesized, **1** is air-stable over a period of several days. In order to study its stability further, electronic absorption spectra of **1** were collected both in solid state and in aqueous solution. Remarkably, the two spectra show the same absorption bands, this fact indicating its stability in aqueous solution (Fig. 2a). SEM-EDAX analysis gave a molar ratio of 1:3 for the Gd/Cl relation in **1** (Fig. 2b).

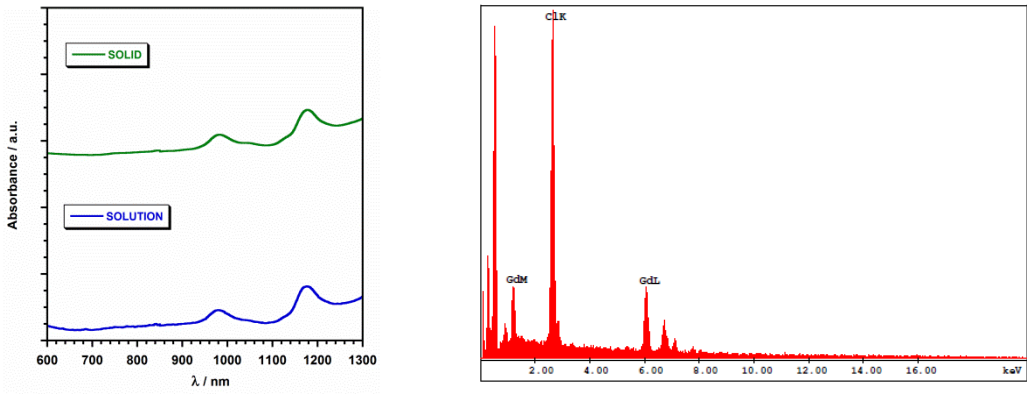

(**a**) (**b**)

Figure 2. (**a**) Electronic absorption spectra from samples of compound **1** in solid state (top) and in aqueous solution (bottom); (**b**) SEM-EDAX spectrum for compound **1**.

Preprints (www.preprints.org) | NOT PEER-REVIEWED | Posted: 26 March 2021 doi:10.20944/preprints202103.0662.v1

3.2. Description of the Crystal Structure

Crystal data and structure refinement parameters are summarized in Table 1. Compound **1** crystallizes in the monoclinic system with space group $P2_1/c$. Its crystal structure is made up of $[Gd(thy)_2(H_2O)_6]^{3+}$ cations, ClO_4^- anions and water molecules of crystallization, which are held together mainly by electrostatic forces and H-bonding interactions. A $[Gd(thy)_2(H_2O)_6]^{3+}$ cation, three ClO_4^- anions and two non-coordinating water molecules are present in the asymmetric unit of **1**.

Table 1. Summary of the crystal data and structure refinement parameters for **1**.

Compound	**1**
CCDC	2009091
Formula	$C_{10}H_{28}N_4O_{24}Cl_3Gd$
M_r/g mol^{-1}	851.96
Crystal system	monoclinic
Space group	$P2_1/c$
a/Å	13.192(1)
b/Å	9.901(1)
c/Å	20.985(1)
α/°	90
β/°	95.18(1)
γ/°	90
V / Å^3	2729.8(2)
Z	4
D_c/g cm^{-3}	2.073
μ(Mo-K$_\alpha$)/mm^{-1}	2.832
Goodness-of-fit on F^2	1.081
R_1 [$I > 2\sigma(I)$]/all	0.0280/0.0325
wR_2 [$I > 2\sigma(I)$]/all	0.0703/0.0733

The Gd^{III} ion in **1** is eight-coordinate and bonded to eight oxygen atoms, two oxygen atoms from carbonyl groups of two thymine ligands and six oxygen atoms of six water molecules (Fig. 1). The average value of the Gd-O bond lengths [2.381(1) Å] is somewhat shorter than that of the Gd-O_{water} bond lengths [2.390(1) Å]. The O-Gd-O bond angles show values covering the range of 70.24(6)-148.57(7)°. These values are in agreement with those reported for other species with a similar Gd^{III} environment [23-25]. In **1**, the thymine molecules are planar and form an angle between them of *ca*. 7.8(1)° with a intramolecular thymine-thymine separation of *ca*. 4.08 Å, that corresponds to the O(1)···O(3) distance. The C−C, C−N, and C−O bond lengths agree with those found in the literature for the thymine molecule [26].

Preprints (www.preprints.org) | NOT PEER-REVIEWED | Posted: 26 March 2021 doi:10.20944/preprints202103.0662.v1

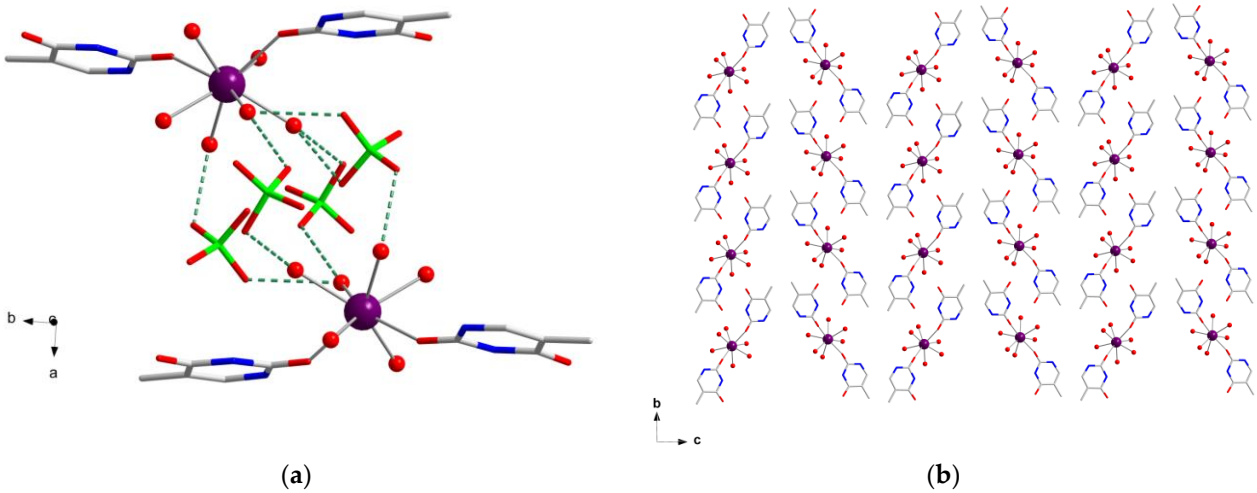

Figure 3. (**a**) View along the crystallographic *c* axis of the H-bonding interactions (green dashed lines) between perchlorate anions (capped sticks model) and $[Gd(thy)_2(H_2O)_6]^{3+}$ cations in **1**. For the sake of clarity, H atoms are omitted and only coordinated water molecules are shown. Color code: purple, Gd; green, Cl; red, O; blue, N; grey, C; (**b**) View along the crystallographic *a* axis of the herringbone type structure of **1**. H atoms, perchlorate anions and non-coordinating water molecules have been omitted for clarity. Color code: purple, Gd; red, O; blue, N; grey, C.

In the crystal packing of **1**, adjacent $[Gd(thy)_2(H_2O)_6]^{3+}$ cations are connected through H-bonding interactions that occur between thymine pairs, linking them into chains [N(3)···O(4a) = 2.763(3) Å and O(2)···N(10a) = 2.785(3) Å; (a) = x, y-1, z], which grow along the *b* crystallographic axis (Table 2). These chains are separated from each other through perchlorate anions, which interact with coordinated water molecules by means of H-bonding interactions involving the following set of atoms: O(3w)···O(11b) [2.944(3) Å; (b) = -x+1, -y+1, -z+1], O(4w)···O(10b) [2.870(3) Å], O(4w)···O(15c) [2.847(3) Å; (c) = -x+1, y-1/2, -z+3/2] and O(5w)···O(12) [2.713(3) Å] (Fig. 3). The chains based on $[Gd(thy)_2(H_2O)_6]^{3+}$ cations are arranged forming a herringbone type structure, generating thymine planes that exhibit an angle of *ca.* 64(1)° (Fig. 3). The shortest Gd···Gd separation is 8.256(1) Å [Gd(1)···Gd(1d) distance; (d) = -x, -y+1, -z+1]. A supramolecular network is generated by additional H-bonding interactions involving coordinated and non-coordinated water molecules, along with weaker C-H···O interactions [the average value of the C···O distance being *ca.* 3.34 Å for C(13)···O(16), C(6)···O(5d) and C(13)···O(11e); (e) = -x+1, y+1/2, -z+3/2], which contribute to stabilizing the crystal structure in **1** (Table 2).

To further analyze the coordination environment and geometry of the Gd^{III} ion in **1**, the SHAPE program was used [27]. In **1**, the single Gd^{III} ion exhibits a coordination number (CN) equal to 8. For Gd(1) a value of 0.307 was obtained and associated with a square antiprism (SAPR) geometry, the next and closer computed value being 1.733, which was assigned to a biaugmented trigonal prism (BTPR) geometry (Table 3). Hence, these calculated values allow us to assign the D_{4d} symmetry to the Gd(1) ion in complex **1** (Table 3).

Table 2. Selected hydrogen-bonding interactions in **1**.[a]

Preprints (www.preprints.org) | NOT PEER-REVIEWED | Posted: 26 March 2021 doi:10.20944/preprints202103.0662.v1

D-H···A	D-H/Å	H···A/Å	D···A/Å	(DHA)/°
N(1)-H(1)···O(8f)	0.880	2.12(1)	2.982(1)	165.4(1)
N(3)-H(3)···O(4a)	0.880	1.89(1)	2.763(1)	175.6(1)
N(10)-H(10)···O(2g)	0.880	1.92(1)	2.785(1)	168.7(1)
O(1w)-H(1wA)···O(7)	0.951	2.05(1)	2.986(1)	168.4(1)
O(1w)-H(1wB)···O(4a)	0.953	1.77(1)	2.677(1)	159.1(1)
O(2w)-H(2wA)···O(2g)	0.948	1.75(1)	2.691(1)	169.2(1)
O(3w)-H(3wA)···O(11b)	0.953	2.07(1)	2.944(1)	151.0(1)
O(3w)-H(3wB)···O(7wf)	0.950	1.76(1)	2.660(1)	156.0(1)
O(4w)-H(4wA)···O(10b)	0.951	2.01(1)	2.870(1)	149.4(1)
O(4w)-H(4wB)···O(15c)	0.953	1.944(1)	2.847(1)	157.4(1)
O(5w)-H(5wA)···O(12)	0.950	1.77(1)	2.713(1)	169.2(1)
O(5w)-H(5wB)···O(14)	0.950	1.87(1)	2.810(1)	169.1(1)
O(6w)-H(6wA)···O(9h)	0.951	2.27(1)	2.939(1)	126.9(1)
O(6w)-H(6wA)···O(7wf)	0.951	2.31(1)	2.986(1)	127.4(1)
O(6w)-H(6wB)···O(8w)	0.953	1.75(1)	2.694(1)	171.9(1)
O(7w)-H(7wB)···O(8wc)	0.961	1.91(1)	2.896(1)	172.5(1)
O(8w)-H(8wA)···O(13)	0.954	1.91(1)	2.855(1)	170.8(1)
O(8w)-H(8wB)···O(15e)	0.953	1.92(1)	2.846(1)	163.9(1)

[a] Symmetry codes: (a) = x, y-1, z; (b) = -x+1, -y+1, -z+1; (c) = -x+1, y-1/2, -z+3/2; (e) = -x+1, y+1/2, -z+3/2; (f) = x, -y+3/2, z-1/2; (g) = x, y+1, z; (h) = -x+1, -y+2, -z+1.

Preprints (www.preprints.org) | NOT PEER-REVIEWED | Posted: 26 March 2021 doi:10.20944/preprints202103.0662.v1

Table 3. Selected values obtained through the SHAPE program for possible geometries with coordination number (CN) equal to 8 and from the structural parameters of complex **1**.[a]

HPY	HBPY	CU	SAPR	TDD	JGBF	JETBPY	BTPR	JSD	TT
23.392	16.322	9.171	0.307	1.913	15.656	28.471	1.733	4.830	10.015

[a] HPY: Heptagonal pyramid (C_{7v}); HBPY: Hexagonal bipyramid (D_{6h}); CU: Cube (Oh); SAPR: Square antiprism (D_{4d}); TDD: Triangular dodecahedron (D_{2d}); JGBF: Johnson gyrobifastigum (D_{2d}); JETBPY: Johnson elongated triangular bipyramid (D_{3h}); BTPR: Biaugmented trigonal prism (C_{2v}); JSD: Snub diphenoid (D_{2d}); TT: Triakis tetrahedron (Td).

3.3. Analysis of the Hirshfeld surfaces

Hirshfeld surfaces of the cationic $[Gd(thy)_2(H_2O)_6]^{3+}$ complex were calculated and its closer intermolecular interactions were analyzed through the *CrystalExplorer* program [28,29]. These surfaces were mapped having into account the distance from a point on the surface to the nearest atom outside (d_e) and inside (d_i) the surface. To overcome limitations relate to the size of atoms, a normalized contact distance (d_{norm}) was also considered [28,29]. For compound **1**, Hirshfeld surfaces are shown in Fig. 4, where the shorter contacts are displayed using red color [30]. Intermolecular O···H contacts between water molecules and between water molecules and carbonyl groups of the thymine molecules are the main interactions detected on the Hirshfeld surface (Fig. 4). The most important O···H contacts are those involving H-bonds between non-coordinated and coordinated water molecules, which are approximately 48% of the complete fingerprint plot, whereas the O···H interactions involving non-coordinated water molecules and carbonyl groups are highlighted from the full fingerprint as *ca*. 19% of the plot. Finally, additional N···H contacts involving non-coordinated water molecules and N-H groups of the thymine molecules only cover approximately 2% of the fingerprint plot (Fig. 4).

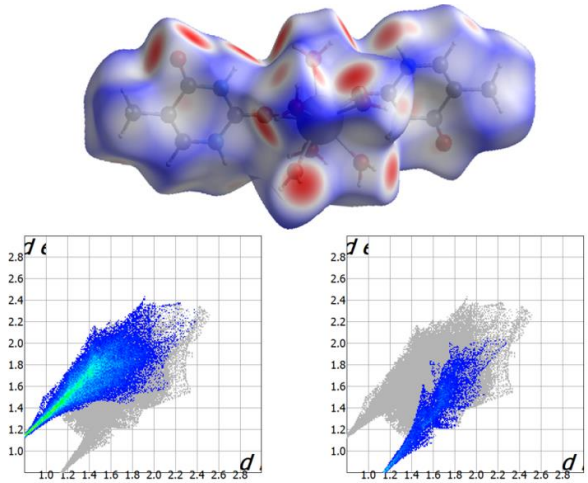

Figure 4. (Top) Hirshfeld surface mapped with d_{norm} function for **1**; (bottom) Fingerprint plots for **1**; (bottom, left) intermolecular O···H contacts between non-coordinated and coordinated water molecules are highlighted from the full fingerprint; (bottom, right) non-coordinated water molecules and thymine carbonyl groups are highlighted from the full fingerprint.

3.4. Magnetic Properties

Dc magnetic susceptibility measurements were carried out on a freshly prepared microcrystalline sample of **1** in the 2-300 K temperature range and under an external magnetic field of 0.5 T. The $\chi_M T$ *versus* T plot (χ_M being the molar magnetic susceptibility per Gd^{III} ion) for compound **1** is given in Fig. 5. At room temperature, the $\chi_M T$ value is *ca*. 7.89 $cm^3mol^{-1}K$, which is very close to that expected for a magnetically isolated Gd^{III} ion ($4f^7$ ion with g_{Gd} = 2.0, S_{Gd} = 7/2 and L_{Gd} = 0). Upon cooling, the $\chi_M T$ value approximately

Preprints (www.preprints.org) | NOT PEER-REVIEWED | Posted: 26 March 2021 doi:10.20944/preprints202103.0662.v1

follows the Curie law to *ca.* 25 K with decreasing temperature, before $\chi_M T$ decreases reaching a minimum value of *ca.* 7.21 $cm^3mol^{-1}K$ at 2 K. The decrease of the $\chi_M T$ value observed for complex **1** would likely be assignable to intermolecular interactions and/or small zero-field splitting (ZFS) effects [31].

To analyze the magnetic behavior and fit the experimental data of the $\chi_M T$ *versus* T plot for complex **1**, the theoretical expression for the magnetic susceptibility of a single and isotropic $S_{Gd} = 7/2$ center was used [$\chi_M = (N\mu_B^2 g_{Gd}^2/3k_B)S_{Gd}(S_{Gd} + 1)/(T - \theta)$] [22,29]. Due to possible intermolecular interactions that can take place in **1**, a θ parameter was also included in this expression. The best least-squares fit gave the parameters g_{Gd} = 2.008(1) and θ = -0.039(1) K with $R = 1.9 \times 10^{-5}$ for **1** {R being the agreement factor defined as $\Sigma_i[(\chi_M T)_i^{obs} - (\chi_M T)_i^{calcd}]^2/[(\chi_M T)_i^{obs}]^2$}.

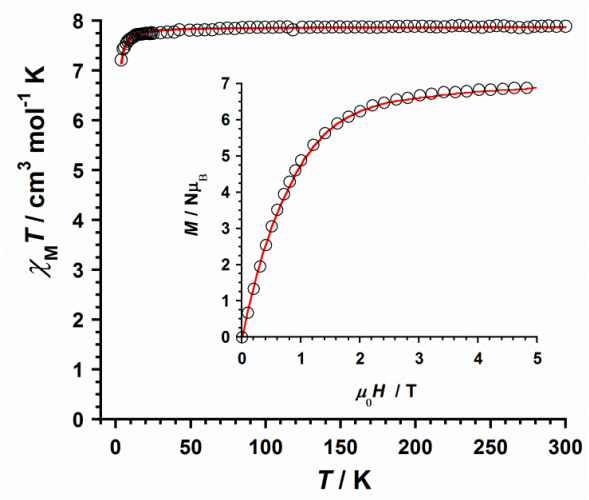

Figure 5. $\chi_M T$ *versus* T plot obtained for compound **1**. The inset shows the field dependence of the molar magnetization (M) plot at 2.0 K for **1**. The solid red lines represent the best fit of the experimental data.

Field dependence of the molar magnetization (M) plot for **1** at 2 K is given in the inset of Fig. 5. This plot exhibits a continuous increase of M with the applied magnetic field, showing a maximum value of M obtained for **1** (*ca.* 6.92 μ_B) at 5.0 T that is as expected for a mononuclear Gd^{III} complex [24]. The experimental data of the M *versus* H plot were close to the Brillouin curve generated with values of g and S of 2.0 and 7/2, respectively (Figure 5) [31].

3.5. MR Imaging Phantom Studies

The relaxometric properties of compound **1** as a potential high-field MR imaging contrast agent were evaluated [32]. 13 samples of **1** were prepared in physiological serum with concentrations covering the range of 0.0-3.2 mM and were measured on a clinical MR scanner (Philips Achieva 3T) by using the volumetric head 8 channels SENSE coil (Fig. 6).

Preprints (www.preprints.org) | NOT PEER-REVIEWED | Posted: 26 March 2021 doi:10.20944/preprints202103.0662.v1

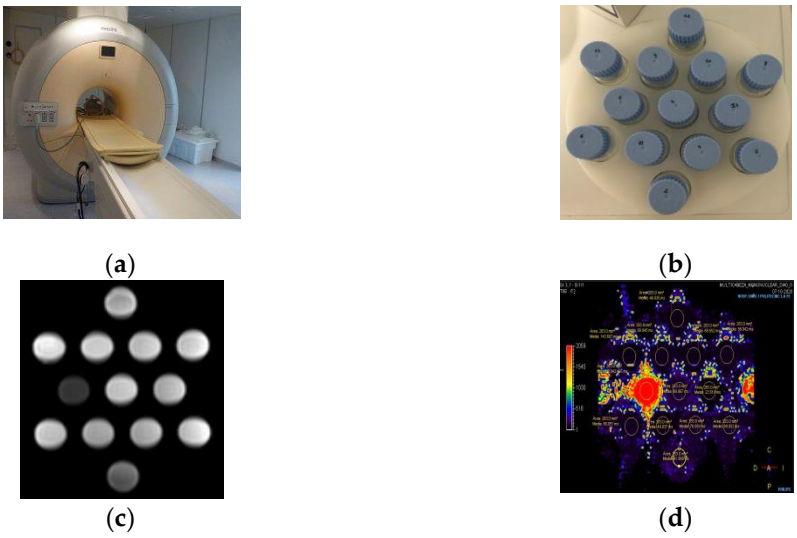

Figure 6. (**a**) MR imaging scanner (Philips Achieva 3T); (**b**) Samples of **1** prepared in physiological serum with concentrations covering the range of 0.0-3.2 mM; (**c**) MR images of the tube phantoms of **1**; (**d**) T_2 parametric map analysis.

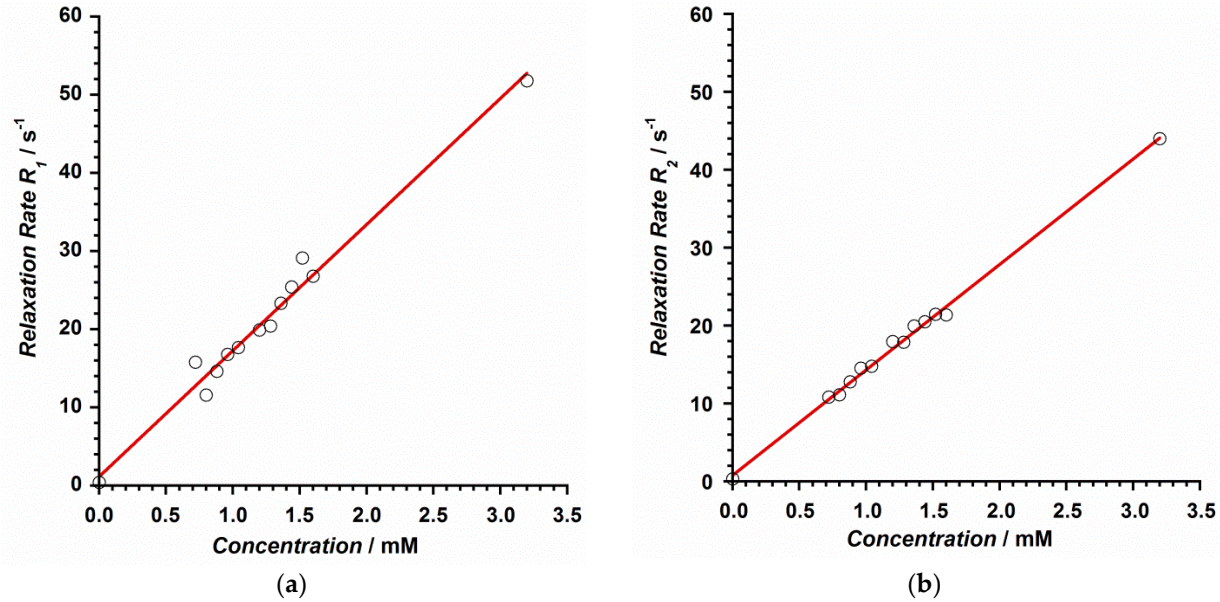

Figure 7. Relaxation rate *versus* contrast concentration plot obtained for the relaxativities r_1 (**a**) and r_2 (**b**) of compound **1**. The red line represents the best linear fit of the experimental data.

The relaxation rate, denoted by R (and expressed in s^{-1}), was obtained for each concentration through the calculation of the corresponding relaxation time T. R_1 was obtained by calculating the T_1 time from FFE sequences with 2°, 5°, 10°, 15°, 25° and 45° flip angles, whereas r_2 and r_2* values were obtained after calculating T_2 and T_2* relaxation times from TSE and GRE sequences with 32 echo times each, TE_1 = 10 ms, ΔTE = 10 ms and TE1 = 0.9 ms, ΔTE = 0.7 ms, respectively [33]. Thus, the longitudinal relaxivity (r_1) of **1** at 3 T was determined to be 16.1 $mM^{-1}s^{-1}$, whereas the transversal relaxivities r_2 and r_2* values were 13.5 and 14.5 $mM^{-1}s^{-1}$, respectively (Figs. 7 and 8). These results show relaxivity values for **1** that are much higher than those of commercial MR imaging contrast agents currently employed on 3 T equipments [32], which make **1** potentially useful.

Preprints (www.preprints.org) | NOT PEER-REVIEWED | Posted: 26 March 2021 doi:10.20944/preprints202103.0662.v1

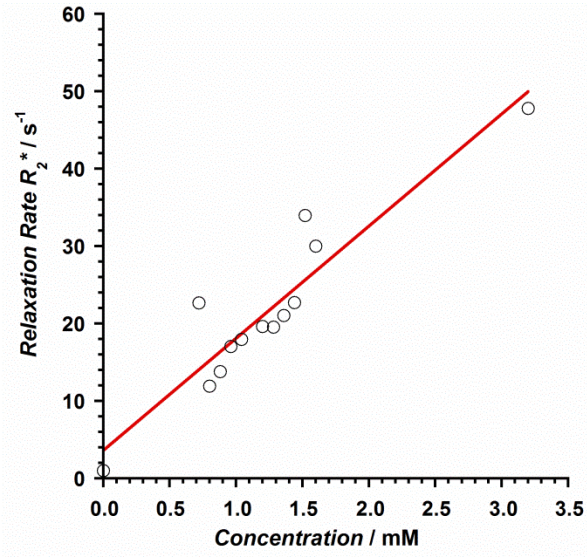

Figure 8. Relaxation rate *versus* contrast concentration plot obtained for the relaxivity r_2* of compound **1**. The red line represents the best linear fit of the experimental data.

4. Conclusions

In summary, the preparation, crystal structure, magnetic properties and MR imaging phantom studies of a novel Gd^{III} complex based on the thymine nucleobase, of formula $[Gd(thy)_2(H_2O)_6](ClO_4)_3{\cdot}2H_2O$ (**1**) [thy = thymine], have been reported. **1** is the first example of compound based on gadolinium and thymine. Given that most of the thymine-containing complexes have been reported with this ligand in form of thyminate anion, we presented in this work a singular strategy to prepare lanthanide systems where the thymine molecule acts as a neutral ligand towards the metal ion. Besides, **1** displays high relaxivity values and, therefore, can be considered as a suitable candidate for further developments and MR analysis.

Supplementary Materials: X-ray crystallographic data in CIF format for compound **1** are available online at www.mdpi.com/xxx/s1.

Author Contributions: L.M.-B. and J.M.-L. conceived the idea and obtained funding for the project. M.O.-A. carried out the synthesis, the X-ray data collection and the calculations through the CrystalExplorer program. S.G.-C. and A.T.-E. performed the acquisition of the MR images, the phantoms and the parametric map analysis. A.T.-E., L.M.-B., I.C. and J.M.-L. analyzed the data associated with all the experiments and wrote the manuscript, which all authors discussed and commented on. All authors have read and agreed to the published version of the manuscript.

Funding: This research was funded by the VLC-BIOMED Program (2017) of the University of Valencia [Subprogram A "*Ayudas para el fomento de acciones coordinadas UV-HUP/IIS La Fe*", Project 11-2017-A] and the Spanish Ministry of Science, Innovation and Universities [Project PID2019-109735GB-I00 and CEX2019-000919-M (Excellence Unit "*María de Maeztu*")].

Institutional Review Board Statement: Not applicable.

Informed Consent Statement: Not applicable.

Data Availability Statement: The reported data are available on request from the corresponding author.

Acknowledgments: The authors thank Dr. Nicolas Moliner for its assistance in SQUID measurements. M.O.A. and J.M.L. thank the Spanish "FPI fellowships" and "Ramón y Cajal" Programmes, respectively.

Conflicts of Interest: The authors declare no conflict of interest.

References

1. Lippert, B.; Sanz Miguel, P.J. The Renaissance of Metal–Pyrimidine Nucleobase Coordination Chemistry. *Acc. Chem. Res*., **2016**, 49, 8, 1537-1545.
2. Somerville, R.L. *Encyclopedia of Genetics*, Academic Press, 2001, pp. 1965-1966.
3. Park, H.J.; Zhang, K.; Ren, Y.; Nadji, S.; Sinha, N.; Taylor, J.-S.; Kang, Ch.H. Crystal structure of a DNA decamer containing a cis-syn thymine dimer. *PNAS*, **2002**, *99*, 15965-15970.
4. Sakate, M.; Hosoda, H.; Suzuki, T. Crystal structures of bis-[2-(pyridin-2-yl)phenyl-κ^2N,C^1]rhodium(III) complexes containing an acetonitrile or monodentate thyminate(1−) ligand. *Acta Cryst.*, **2016**, E*72*, 543-547.
5. Vegas, V.G.; Lorca, R.; Latorre, A.; Hassanein, K.; Gómez-García, C.J.; Castillo, O.; Somoza, A.; Zamora, F.; Amo-Ochoa, P. Copper(II)-Thymine Coordination Polymer Nanoribbons as Potential Oligonucleotide Nanocarriers. *Angew. Chem. Int. Ed*., **2017**, *56*, 987-991.
6. Correa, R.S.; Freire, V.; Barbosa, M.I.F.; Bezerra, D.P.; Bomfim, L.M.; Moreira, D.R.M.; Soares, M.B.P.; Ellena, J.; Batista, A.A. Ru(II)–thyminate complexes: new metallodrug candidates against tumor cells. *New J. Chem*., **2018**, *42*, 6794-6802.
7. Silva, S.L.R.; Baliza, I.R.S.; Dias, R.B.; Sales, C.B.S.; Rocha, C.A.G.; Soares, M.B.P.; Correa, R.S.; Batista, A.A.; Bezerra, D.P. *Sci. Rep*., **2019**, *9*, 11094.
8. De, H.; Paul, A.; Datta, A. Theoretical study of Au_4 thymine, Au_{20} and Ag_{20} uracil and thymine complexes for surface enhanced Raman scattering. *Comput. Theor. Chem*., **2017**, *1111*, 1-13.
9. Kondo, J.; Yamada, T.; Hirose, C.; Okamoto, I.; Tanaka, Y.; Ono, A. Crystal structure of metallo DNA duplex containing consecutive Watson-Crick-like T-Hg(II)-T base pairs. *Angew. Chem. Int. Ed*., **2014**, *24*, 2385-2388.
10. Yamaguchi, H.; Šebera, J.; Kondo, J.; Oda, S.; Komuro, T.; Kawamura, T.; Dairaku, T.; Kondo, Y.; Okamoto, I.; Ono, A.; Burda, J.V.; Kojima, C.; Sychrovský, V.; Tanaka, Y. The structure of metallo-DNA with consecutive thymine–Hg^{II}–thymine base pairs explains positive entropy for the metallo base pair formation. *Nucleic Acids Res*., **2014**, *42*, 4094-4099.
11. Kuriyama, M.; Haruta, K.; Dairaku, T.; Kawamura, T.; Kikkawa, S.; Inamoto, K.; Tsukamoto, H.; Kondo, Y.; Torigoe, H.; Okamoto, I.; Ono, A.; Morita, E.H.; Tanaka, Y. Hg^{2+}-Trapping Beads: Hg^{2+}-Specific Recognition through Thymine–Hg(II)–Thymine Base Pairing. *Chem. Pharm. Bull*., **2014**, *62*, 709-712.
12. Li, L.; Wen, Y.; Xu, L.; Xu, Q.; Song, S.; Zuo, X.; Yan, J.; Zhang, W.; Liu, G. Development of mercury (II) ion biosensors based on mercury-specific oligonucleotide probes. *Biosens. Bioelectron*., **2016**, *75*, 433-445.
13. Chun, H.J.; Kim, S.; Han, Y.D.; Kim, D.W.; Kim, K.R.; Kim, H.S.; Kim, J.H.; Yoon, H.C. Water-soluble mercury ion sensing based on the thymine-Hg^{2+}-thymine base pair using retroreflective Janus particle as an optical signaling probe. *Biosens. Bioelectron*., **2018**, *104*, 138-144.
14. Kashima, A.; Sakate, M.; Ota, H.; Fuyuhiro, A.; Sunatsukia, Y.; Suzuki, T. Thyminate(2−)-bridged cyclic tetranuclear rhodium(III) complexes formed by a template of a sodium, calcium or lanthanoid ion. *Chem. Commun*., **2015**, *51*, 1889-1892.
15. Armentano, D.; Marino, N.; Mastropietro, T.F.; Martínez-Lillo, J.; Cano, J.; Julve, M.; Lloret, F.; De Munno, G. Self-Assembly of a Chiral Carbonate- and Cytidine-Containing Dodecanuclear Copper(II) Complex: a Multiarm-Supplied Globular Capsule. *Inorg. Chem*., **2008**, *47*, 10229-10231.
16. Martínez-Lillo, J.; Mastropietro, T.F.; Lappano, R.; Madeo, A.; Alberto, M.E.; Russo, N.; Maggiolini, M.; De Munno, G. Rhenium(IV) compounds inducing apoptosis in cancer cells. *Chem. Commun*., **2011**, *47*, 5283-5285.
17. Marino, N.; Armentano, D.; Mastropietro, T.F.; Julve, M.; De Munno, G.; Martínez-Lillo, J. Cubane-Type Cu^{II}_4 and $Mn^{II}_2Mn^{III}_2$ Complexes Based on Pyridoxine: A Versatile Ligand for Metal Assembling. *Inorg. Chem*., **2013**, *52*, 11934-11943.
18. Armentano, D.; Barquero, M.A.; Rojas-Dotti, C.; Moliner, N.; De Munno, G.; Brechin, E.K.; Martínez-Lillo, J. Enhancement of Intermolecular Magnetic Exchange through Halogen···Halogen Interactions in Bisadeninium Rhenium(IV) Salts. *Cryst. Growth Des*., **2017**, *17*, 5342-5348.
19. Orts-Arroyo, M.; Castro, I.; Lloret, F.; Martínez-Lillo, J. Field-induced slow relaxation of magnetisation in two one-dimensional homometallic dysprosium(III) complexes based on alpha- and beta-amino acids. *Dalton Trans*., **2020**, *49*, 9155-9163.
20. Orts-Arroyo, M.; Castro, I.; Martínez-Lillo, J. Detection of Hypoxanthine from Inosine and Unusual Hydrolysis of Immunosuppressive Drug Azathioprine through the Formation of a Diruthenium(III) System. *Biosensors*, **2021**, *11*, 19.
21. SHELXL-2018/1, Bruker Analytical X-ray Instruments, Madison, WI, 2018.
22. DIAMOND 4.5.0, Crystal Impact GbR, CRYSTAL IMPACT, 2018.
23. Guillou, O.; Bergerat, P.; Kahn, O.; Bakalbassis, E.; Boubekeur, K.; Batail, P.; Guillot, M. Ferromagnetically coupled gadolinium(III)copper(II) molecular material. *Inorg. Chem*., **1992**, *31*, 110-114.
24. Cañadillas-Delgado, L.; Fabelo, O.; Cano, J.; Ruiz-Pérez, C. *Magnetic Interactions in oxo-carboxylate bridged Gadolinium(III) Complexes Synthesis, Crystal Structures and Magnetic Properties*, Nova Science Publishers, Inc. 400 Oser Avenue, Suite 1600, Hauppauge, NY, USA, 2010.
25. Martínez-Lillo, J.; Cañadillas-Delgado, L.; Cano, J.; Lloret, F.; Julve, M.; Faus, J. A heteropentanuclear oxalato-bridged [$Re^{IV}_4Gd^{III}$] complex: synthesis, crystal structure and magnetic properties. *Chem. Commun*., **2012**, *48*, 9242-9244.
26. Portalone, G.; Bencivenni, L.; Colapietro, M.; Pieretti, A.; Ramondo, F. The Effect of Hydrogen Bonding on the Structures of Uracil and Some Methyl Derivatives Studied by Experiment and Theory. *Acta Chem. Scand*., **1999**, *53*, 57-68.
27. SHAPE 2.1, Llunell, M.; Casanova, D.; Cirera, J.; Alemany, P.; Alvarez, S. Universitat de Barcelona, Barcelona, Spain, 2013.
28. Spackman, M.A.; Jayatilaka, D. Hirshfeld surface analysis. *CrystEngComm*, **2009**, *11*, 19-32.

 doi:10.20944/preprints202103.0662.v1

29. CrystalExplorer 17, Turner, M.J.; McKinnon, J.J.; Wolff, S.K.; Grimwood, D.J.; Spackman, P.R.; Jayatilaka, D.; Spackman, M.A. University of Western Australia, Perth, Australia, 2017.
30. Orts-Arroyo, M.; Castro, I.; Lloret, F.; Martínez-Lillo, J. Molecular Self-Assembly in a Family of Oxo-Bridged Dinuclear Ruthenium(IV) Systems. *Cryst. Growth Des*., **2020**, *20*, 2044-2056.
31. Kahn, O. *Molecular Magnetism*, VCH, New York, 1993.
32. Mousavi, B., Chauvin, A.-S.; Moriggi, L.; Helm, L. Carbazole as Linker for Dinuclear Gadolinium-Based MRI Contrast Agents. *Eur. J. Inorg. Chem*. **2017**, 5403-5412.
33. Rohrer, M.; Bauer, H.; Mintorovitch, J.; Requardt, M.; Weinmann, H.-J. Comparison of magnetic properties of MRI contrast media solutions at different magnetic field strengths. *Invest. Radiol*. **2005**, *40*, 715-724.